Harnessing Labile Bonds between Nanogel Particles to Create Self-Healing Materials

German V. Kolmakov,[†] Krzysztof Matyjaszewski,[‡] and Anna C. Balazs[†,*]

[†]Chemical Engineering Department, University of Pittsburgh, Pittsburgh, Pennsylvania 15261 and [‡]Department of Chemistry, Carnegie Mellon University, Pittsburgh, Pennsylvania 15213

ABSTRACT Using computational modeling, we demonstrate the self-healing behavior of novel materials composed of nanoscopic gel particles that are interconnected into a macroscopic network by both stable and labile bonds. Under mechanical stress, the labile bonds between the nanogels can break and readily re-form with reactive groups on neighboring units. This breaking and re-forming allows the units in the network to undergo a structural rearrangement that preserves the mechanical integrity of the sample. The simulations show that just a small fraction of labile bonds leads to a roughly 25% increase in the stress needed to induce fracture. Thus, the labile bonds can significantly improve the tensile strength of the material. The findings provide guidelines for creating high-strength, self-healing materials.

KEYWORDS: self-healing materials · cross-linked nanogels · particle gels · deformable particles · computer simulations

One of the critical issues that researchers must address in fabricating new devices and components is establishing approaches for enhancing the sustainability of the structures. One potential means of meeting this challenge is to create materials that have the ability to "autonomously" sense and respond to damage and wear in a beneficial way.[1−3] For instance, by imparting self-healing mechanisms into coatings, both the surface and the entire underlying system could be protected from mechanical deformation and, thus, the life span of the system could be extended. A particularly useful way of introducing the self-healing behavior would be to harness the mechanical deformations that the material experiences in the course of its use as the actual agent for the self-repair.[4] Consider, for example, that continued mechanical stress can lead to bond breaking, which can expose new chemical reactivity within the material. The challenge is to design materials that could exploit this chemical reactivity to effectively strengthen the system. Such materials would form self-sufficient, synthetic systems that respond to the damage with little or no human intervention.

Herein, we use computational modeling to design a gel coating that undergoes structural rearrangement in response to mechanical stress and thereby prevents the catastrophic failure of the material. The primary building blocks in our system are nanoscopic polymer gel particles, or "nanogels". Conceptually, this work was inspired by recent experiments on the synthesis of nanogel particles with well-controlled sizes.[5,6] Furthermore, the surface of these particles can be functionalized with various reactive groups, which allow the individual nanogel particles to be cross-linked into a macroscopic material.[5−8] The cross-linkers can include both stable bonds and labile moieties (*e.g.*, thiol groups that enable thiol/disulfide exchange reactions).[5−8] Thus, the systems can exhibit a "dual cross-linking", being interconnected by both reactive and nonreactive linkages.

Motivated by these developments in chemical synthesis, we simulate nanogel particles that are connected *via* a fraction of labile bonds and a fraction of stronger, less reactive bonds, which we refer to as the "permanent" bonds. (Here, the labile linkages could represent hydrogen bonds,[9] as well as the thiol or disulfide units noted above, while the permanent links could model C−C bonds.) Once a permanent bond is broken, it is reconnected at a significantly slower rate than the reactive, labile bonds (as detailed in the Methodology section). In this manner, our material also exhibits a dual cross-linking.

Within this system, the stable, permanent bonds between the nanogels play an essential role by imparting structural

*Address correspondence to balazs@pitt.edu.

Received for review January 19, 2009 and accepted March 18, 2009.

Published online March 26, 2009.
10.1021/nn900052h CCC: $40.75

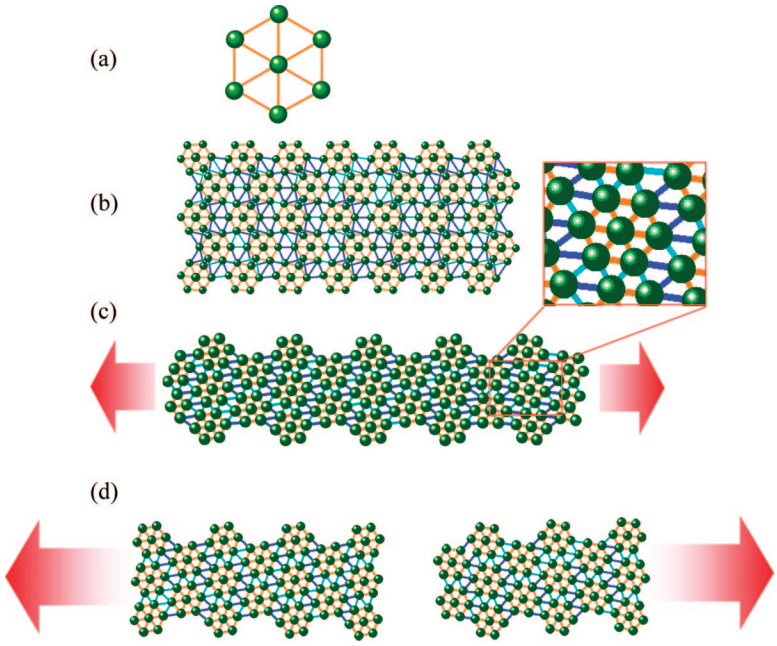

Figure 1. (a) Schematic of a deformable gel particle; each particle consists of seven nodes (green points) connected by springlike bonds (orange lines). (b–d) Graphical output from simulations for sample with $P = 0.8$. (b) Fragment of an undeformed nanogel layer. Dark blue lines mark stable bonds between clusters and light blue lines indicate labile bonds. (c) Plastically deformed layer shown in panel b after the structural rearrangement due to a tensile force (shown by horizontal red arrows); here $\sigma = \sigma_1 = 1.05\sigma^*$ ($\sigma_{cr1} < \sigma_1 < \sigma_{cr2}$). the inset shows an enlargement of a fragment of the gel. (d) Fracture of the layer at $\sigma = \sigma_2 = 1.29\sigma^*$ ($\sigma_2 > \sigma_{cr2}$) (see text for notations).

integrity. As we show below, it is the reactive, labile bonds, however, that improve the strength of the material. In particular, when the material is stressed and deformed, the labile bonds break before the stronger connections; these broken bonds allow the particles to slip and slide, come into contact with new neighbors, and make new connections that maintain the continuity of the film. In this manner, the labile bonds impart self-healing properties to the material. Through the computer simulations, we pinpoint the parameter range for optimizing this self-healing behavior. In fact, we find that just a relatively small volume fraction of labile bonds within the material can dramatically increase the ability of the network to resist catastrophic failure.

The specific predictions described below could be tested through physical experiments on the dual cross-linked systems described in refs 5−8. Furthermore, Creton *et al.*[10] have recently synthesized so-called "soft−soft" nanocomposites involving nanoscopic viscoelastic particles that are cross-linked through an elastic network. In the latter system, the cross-linkers are chemically uniform; however, the synthetic approach could potentially be modified to include additional components and, in this manner, exhibit the dual cross-linking motif described herein.

We note that such a network of associated colloidal particles is commonly referred to a "particle gel". To the best of our knowledge, there have been no prior computational studies on particle gels where each individual particle is itself a deformable gel. Thus, the studies presented here represent the first simulations of a deformable network where each unit can itself undergo deformation.

RESULTS AND DISCUSSION

In the simulations, the interconnected gel particles form a two-dimensional network (see Figure 1). Given that N_{sta} and N_{labile} are the respective average number of stable and labile bonds in the system, we use the ratio $P = N_{sta}/(N_{sta} + N_{labile})$ to characterize the interconnections in the network. For example, for $P = 1$, the nanogel particles are interconnected solely by the stable bonds; for $P = 0.8$, the material encompasses 20% labile bonds.

To probe the effect of the labile bonds on the system's response to deformation, we applied a tensile force (along X) at the edges of the layer, as shown in Figure 1. We initially considered samples composed of five rows of gel particles, with 10 particles in each row. The data in Figures 2 and 3 were obtained by averaging over six independent simulations. The temperature was set to room temperature, $T = 300$ K.

We define the tensile stress σ as the ratio of the tensile force to the cross section (in the Y direction) of the unperturbed layer (*i.e.*, we calculate the engineering stress).[11] Due to the applied stress, the sample becomes stretched and the sample length, L, becomes greater than its initial value of L_0. In Figure 2, we plot (L/L_0) at $P = 0.8$ for three values of σ; each value typifies one of the three regimes shown in the phase map in Figure 3. Note that σ is specified with respect to σ^*, which is the minimal stress at which the $P = 1$ sample completely fractures into two or more separate pieces. The tensile force was applied in a quasi-static manner so the stress reaches its full, specified value at $t = 500$ (in simulation time steps). At the smallest of the

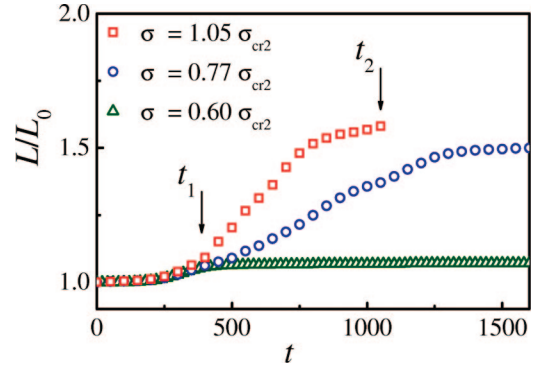

Figure 2. Dependence of the normalized length of the small sample, L/L_0, on time t. The moment t_1 at which plastic deformation of the sample starts and the moment t_2 at which the sample fractures into two pieces (Figure 1d) are labeled by arrows.

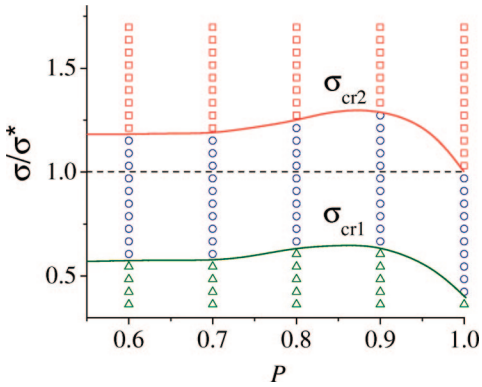

Figure 3. Phase map that indicates the regions where the stretched gel layer exhibits elastic (green triangles) and plastic (blue circles) deformation, and fracture (red boxes). The regions are divided by the first (σ_{cr1}) and second (σ_{cr2}) critical lines. Points show the results from the simulations. Vertical line $P = 1$ corresponds to a permanently cross-linked sample: $P < 1$ corresponds to dual cross-linked sample. σ^* is the minimal stress at which the $P = 1$ sample fractures.

applied stresses, the green curve indicates that the system displays an elastic deformation, that is, the film resumes its initial dimensions after the tensile force is removed. After the transient process that occurs during $t < 500$, the sample reaches a new stationary, stretched state with a slightly longer L.

The blue curve in Figure 2 is characteristic of plastic deformation (area filled with blue circles in Figure 3), where the system undergoes permanent change and does not resumes its shape after the tension is released. The time at which structural rearrangement in this sample takes place, t_1, is marked by an arrow. It is clearly seen that at $t > t_1$, the length of the sample is significantly increased, and Figure 1c shows the new, stable steady state that is formed at $t > 1300$.

Finally, the red curve in Figure 2 reveals the behavior of the material at the highest value of σ. Here, the sample fractures (see Figure 1d) at the time marked t_2. Note that directly prior to t_2 the slope of the curve increased in a step-like manner. For $t > t_2$, the two pieces of the sample move apart in opposite directions under the action of the tensile force.

Through these simulations, we generated the plot in Figure 3, which maps the response of the system to the applied deformation in terms σ and P. (Note that σ is normalized by σ^*.) To carefully pinpoint the locations of the boundaries in this phase map, we carried out six independent runs for each point. The size of the error bars is equal to the vertical distance between two nearest points on a given vertical line. For this small sample, there is a sharp separation between the regions of elastic (green triangles) and plastic (blue circles) deformation; this separation is marked by the line labeled σ_{cr1} in Figure 3. Similarly, there is a sharp separation between the regions where the sample deforms plastically (blue circles) and exhibits a catastrophic failure (red boxes); this separation is marked by the line labeled σ_{cr2}.

For samples within the elastic region ($\sigma < \sigma_{cr1}$ in the plot), we can calculate the Young's modulus as $E = \sigma L_0/\Delta L$, where $\Delta L/L_0$ is the relative elongation of the sample. We found that E was independent of P. Additionally, up to the first critical stress σ_{cr1}, E was roughly independent (with an accuracy of $\pm 5\%$) of the applied stress.

If the applied tensile stress σ exceeds the yield stress, σ_{cr1}, but is less than the second critical value σ_{cr2}, the sample undergoes plastic deformation, which involves a permanent structural rearrangement within the layer. During the rearrangement, the relative positions of the gel units are changed, as seen in Figure 1c (and Figure 6). While 10−30% of the stable bonds are ruptured for cases with $0.6 \leq P \leq 1$, the labile bonds are re-formed and help maintain the integrity of the layer. At $\sigma > \sigma_{cr2}$, the sample fractures into two sections (at small positive values of $(\sigma - \sigma_{cr2})$), as shown in Figure 1d or a few pieces (at $(\sigma - \sigma_{cr2}) > 0.2\sigma_{cr2}$).

As is evident from Figure 3, both the first and second critical stresses, σ_{cr1} and σ_{cr2}, depend on P, that is, the fraction of labile bonds. Moreover, the second critical stress σ_{cr2} increases by approximately 30% if P is reduced from 1 (or 100% stable bonds) to $P = 0.9$, where 10% of bonds between gel particles were designated as labile. This observation indicates that the presence of labile bonds strengthens the material.

A local maximum is clearly seen in the σ_{cr2} (P) curve. At $P < 0.9$, the effect of strengthening by this "dual cross-linking" is partially reduced; this is probably due to a relative weakening of the sample with a reduction in the number of stable bonds. Nonetheless, Figure 3 demonstrates that, for $0.6 < P < 1$, the second critical stress σ_{cr2} of the dual cross-linked nanogel exceeds the critical stress $\sigma^* \equiv \sigma_{cr2}$ ($P = 1$) for the sample with purely stable cross-links. In other words, the breaking and re-forming of labile bonds (*i.e.*, the "self-healing" of the material) enables the system to withstand higher stresses than a material that is cross-linked by purely stable bonds.

While the thin sample described above illustrates the response of the dual cross-linked material to the deformation, we simulated larger samples and carried out a Weibull statistical analysis[12] on these samples to further characterize the behavior of our system. In particular, we examined samples that encompassed eight rows of gel particles, with 10 particles in each row, and a sample with 12 rows, where each row consisted of 15 particles. In the thinner sample in Figure 1, a certain fraction of the labile bonds were located in the outer surface of the film. When the tensile deformation was applied, some of these bonds were readily broken (as they have fewer neighbors to bind them), and this process effectively nucleated a small surface crack, which then initiated the dynamic processes described above. As the width of the sample is increased, however, the relative fraction of surface bonds decreases. To ensure

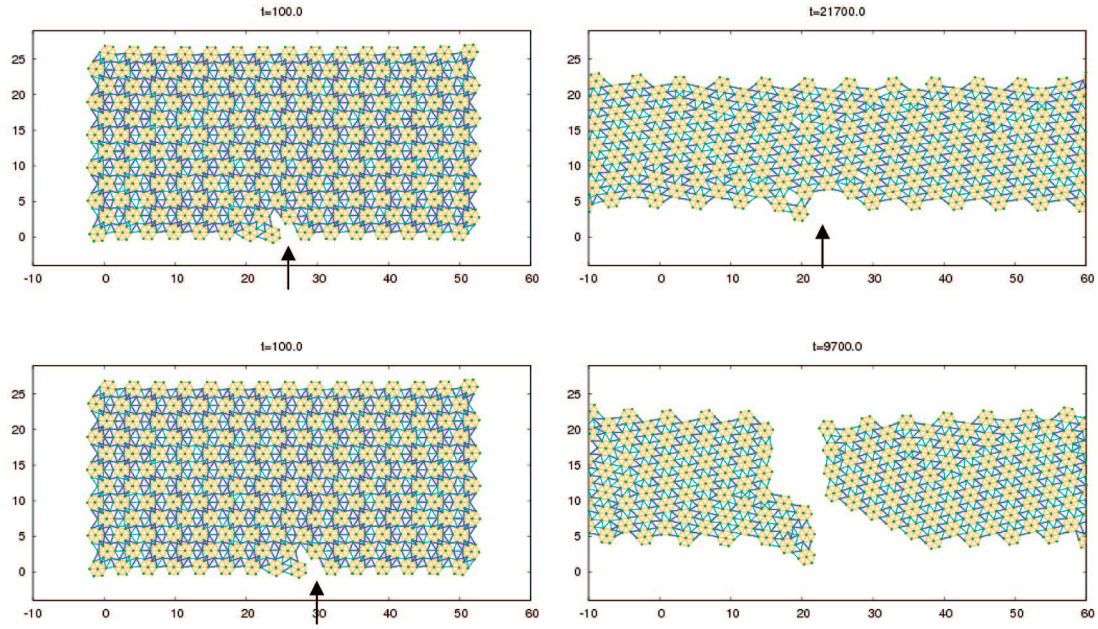

Figure 4. Two different realizations of a large sample, which is composed of 12 rows of gel clusters, with 15 clusters in a row. The initial cracks are marked by arrows. The dual cross-linking ratio is $P = 0.8$. (Top) The sample is stable for 2100 time steps before a structural rearrangement takes place. (Bottom) The sample fractures at $t \sim 9700$. It is clearly seen that the fracture is initiated at the crack.

that the simulations run in realistic time scales, for the larger samples, we initially introduce a small crack at a random site at the surface and then carry out the analysis described below.

After a crack was introduced at the lower surface (an example is shown by the arrow on Figure 4), the sample was stretched by a tensile force. We then determined whether or not the sample fractures after being stretched at given stress σ. The simulation was repeated eight times, with different initial positions for the crack. The probability of rupture, p_b, was calculated as a ratio of the number of times the sample was completely fractured, n_b, to the total number of attempts, n_{tot} ($p_b = n_b/n_{tot}$).

In the Weibull statistical analyses, the probability of a sample breaking is described by the two-parameter cumulative distribution function

$$p_b(\sigma) = 1 - \exp[-(\sigma/\sigma_b)^m] \quad (1)$$

where σ_b and m are the fitting parameters characterizing the distribution. The parameter σ_b is the characteristic stress at which the sample fractures, and the exponent m characterizes the brittleness of the sample. (Note that $\sigma_b \equiv \sigma_{cr2}$ in Figure 3.)

The results of the analysis for the two larger samples are quantitatively similar, and thus, we present the data for the largest sample in Figure 5. The plot in Figure 5a displays the dependence of the probability of rupture, p_b, on the applied stress σ for a sample with $P = 0.8$; each red point represents an average of eight independent simulations. The stress σ is normalized by the stiffness of the bond, κ (see Methodology), which has the same dimensionality as σ in two dimensions (so that the

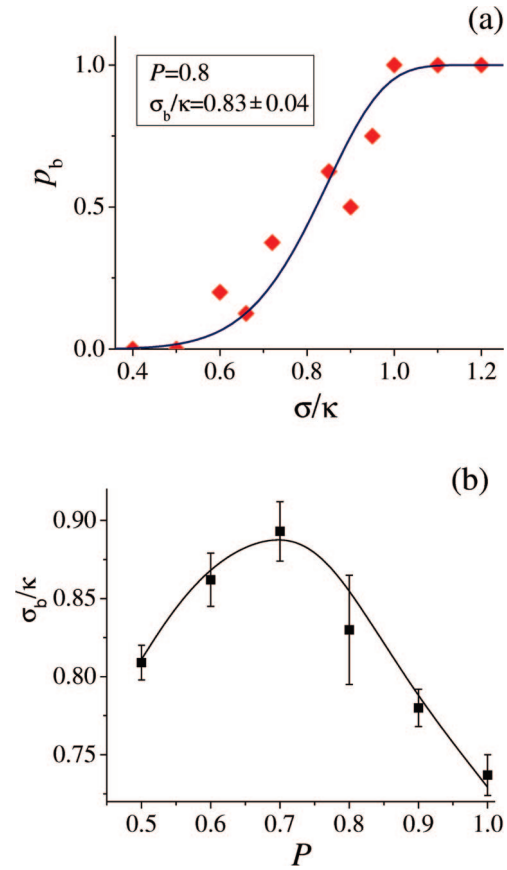

Figure 5. (a) Probability for the sample to break p_b, plotted as a function of the applied tensile stress σ. Red diamonds show the results from the simulations for dual cross-linked samples with $P = 0.8$. Blue curve shows the results of fitting of the data by the Weibull probability distribution function. The stress is normalized by the bond stiffness constant κ. (b) Dependence of σ_b on the dual cross-linking ratio P as calculated through Weibull statistical analyses for the largest sample.

ratio σ/κ is dimensionless). The blue curve shows the result of fitting the numerical data to the function $p_b(\sigma)$ in eq 1. The fitting parameters were determined with the aid of the least-squares method. The values for the relevant parameters are $\sigma_b/\kappa = 0.83(\pm 0.04)$ and $m = 5.15(\pm 0.04)$ for $P = 0.8$. Thus, the statistical error in determination of the fitting parameters is ~5% for the characteristic rupture stress σ_b and less than 1% for the exponent m. It is seen that for $P = 0.8$, the curve characterizing p_b exhibits a gentle slope.

By generating plots similar to Figure 5a for different values of P, we obtain the curve in Figure 5b, which shows the dependence of the characteristic rupture stress σ_b on the dual cross-linking ratio P. The error bars in this plot show the standard deviations for σ_b obtained *via* the fitting procedure. A maximum in the plot is clearly seen at $P \sim 0.7$, showing general agreement with the phase map generated from the thinner sample (see Figure 3). The shift in the position of the maximum in the $\sigma_b(P)$ curve in Figure 5b relative to the position of the maximum in $\sigma_{b2}(P)$ curve in Figure 3 can be attributed to the stronger influence of the boundaries for the smaller sample (*i.e.*, the fraction of the clusters at the sample's surface is higher for the smaller sample).

To more completely characterize the behavior of this dual cross-linked material under tensile deformation and to demonstrate its self-healing properties, we also calculated the stress−strain curves. In contrast to calculations described above where a constant stress was applied to a sample, in this study, the sample was stretched at a constant velocity, and the tensile stress was computed as a function of the strain, $\varepsilon = (L - L_0)/L_0$. (In particular, the right edge of the sample was held fixed, while the left edge was displaced along the horizontal axes with a speed V_t.) This type of measurement is widely used in the characterization of cross-linked polymers.[13,14] At the regions of high strain, where structural rearrangement takes place, the true stress is higher that the calculated engineering stress due to the decrease of the sample's cross section in the course of the rearrangement. Thus, these calculations give an estimate from below for the stability region of materials encompassing labile bonds ($P < 1$).

Figure 6 shows the stress−strain curves calculated for the largest sample for $P = 1$ and $P = 0.8$. The tensile speed was equal to $V_t = 10^{-3} \times d/\tau$, where $d = 2\Delta$ is a characteristic size of the cluster. The parameter $\tau = 1/\mu\kappa$ is the elastic response time for a bond, where μ is the mobility of the nodes and κ is the stiffness of the bonds (see below and Methodology section). The first peak at $\varepsilon \approx 0.08$ gives the yield stress. At stresses below the yield stress, the curves for the permanent and dual cross-linked samples coincide with each other. The

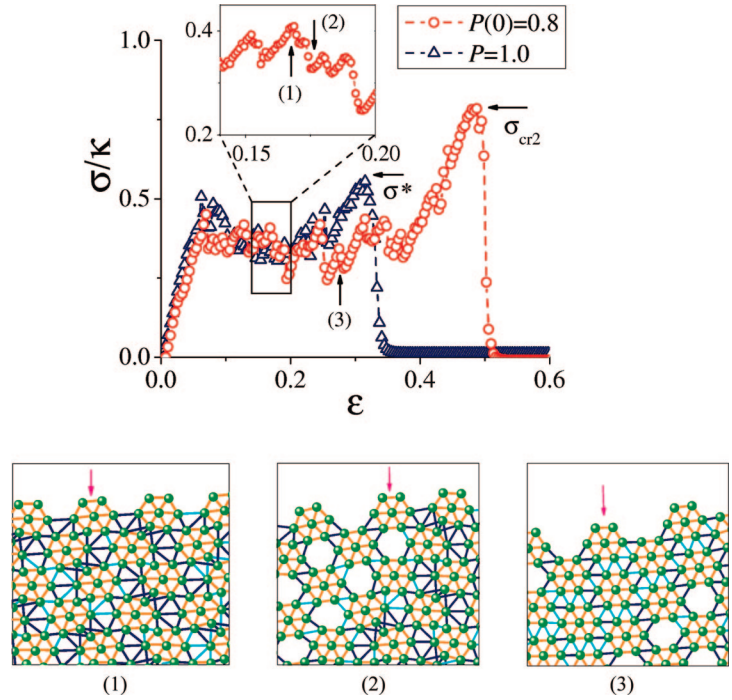

Figure 6. (Top) Stress−strain curve calculated for the largest sample. Stress is normalized by the bond stiffness constant κ. Red circles mark the results for dual cross-linked samples $P(0) = 0.8$; blue triangles indicate the results for the permanently cross-linked $P = 1$ samples. Dashed curves are plotted as to guide the eye. The stress σ^* at which a permanently cross-linked sample fractures and the stress σ_{cr2} at which a dual cross-linked sample with initially 20% of labile bonds fractures are marked by horizontal arrows. Inset shows jumps in the stress−strain curve in an enlarged scale. (Bottom) Panels showing the evolution of a portion of the sample with the increasing strain ε. The moments of time at which the panels are plotted are labeled in the upper plot by vertical arrows. Panels 1 and 2 show the respective images of the sample just before and after the formation of holes between the gel particles because of the bond rupture and panel 3 shows that sample after the holes have collapsed at a later time. A cluster positioned near these structural rearrangements is marked by a verticle arrow.

latter behavior arises because the stiffness constants for the strong and labile bonds are chosen to be equal. Panels 1−3 in Figure 6 illustrate the mechanism of structural rearrangement (plastic elongation) of the sample for $\varepsilon > 0.08$. As is apparent from panels 1 and 2, the elongation of the sample at $\varepsilon > 0.08$ is accompanied by the rupture of bonds and the formation of holes in the bulk of the sample. (The formation of holes during the plastic deformation of solid samples was also observed in MD simulations in cross-linked polymers.)[13−15] The bond rupture is also responsible for oscillations seen in the stress−strain curves and clearly visible in the inset. In the case of the dual cross-linked sample, the holes collapse at later times due to the formation of new labile bonds between the clusters, as is evident from panel 3 (see also Figures 1c and 4).

It is clearly seen in Figure 6 that the strain at which the $P = 0.8$ dual cross-linked sample fractures ($\varepsilon_b \approx 0.5$) is approximately 1.5 times greater than that for the sample with $P = 1.0$ ($\varepsilon_b \approx 0.33$). The fact that $\sigma_{cr2}(P) > \sigma^*$ for $P = 0.8$ is in agreement with the plot on Figure 3, obtained from simulations involving constant applied stress. These two observations support our con-

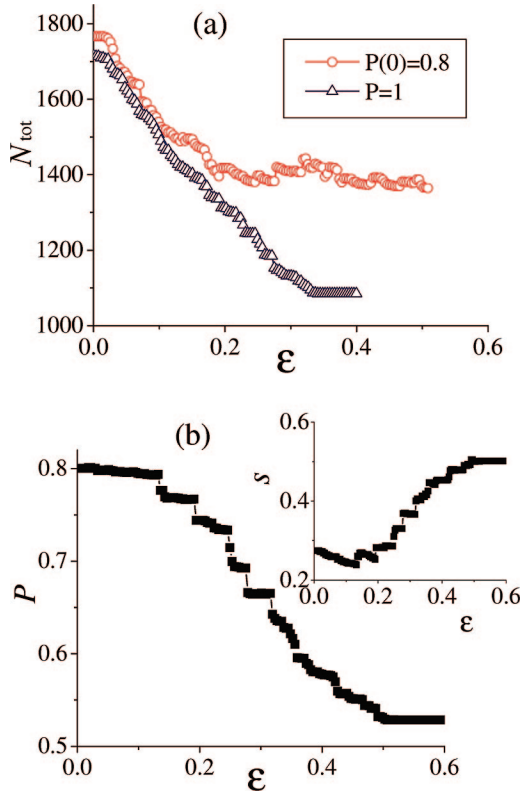

Figure 7. (a) Changes in the total number of bonds in the sample at the initial cross-linking ratio $P(0) = 0.8$ (red circles) and at $P = 1.0$ (blue triangles) during the deformation shown in Figure 6. (b) Dependence of P on strain ε calculated for the same simulation. The inset shows saturation s in the labile bond network as a function of strain.

clusion that the introduction of labile bonds leads to an increase in the mechanical stability of the nanogel material. It is also noteworthy that the area under the curve for the $P = 0.8$ case is greater than that for the $P = 1.0$ sample. Thus, the labile bonds also increase the toughness of the material. These observations show qualitative agreement with the findings in refs 9 and 13 on the behavior of cross-linked polymers; namely, the presence of re-formable bonds (*i.e.*, hydrogen[9] or ionic bonds[13]) leads to an improvement in both the strength and toughness of the materials.

Figure 7a reveals how the total number of bonds in the sample, $N_{tot} = N_{labile} + N_{sta}$, vary with the applied strain for the tensile deformation shown on Figure 6. The data are plotted up to the point where the samples undergo fraction: $\varepsilon \approx 0.5$ for $P = 0.8$ and $\varepsilon \approx 0.33$ for $P = 1.0$. While the total number of bonds decreases during the deformation for both $P = 0.8$ and $P = 1.0$ samples, the total number of bonds for the dual cross-linked sample is always higher than that for the permanently cross-linked sample in the plastic deformation region $\varepsilon > 0.08$. This difference is due to formation of new labile bonds (which were initially ruptured) in the course of the structural rearrangement.

To further characterize the changes in the network during the rearrangement in the dual cross-linked

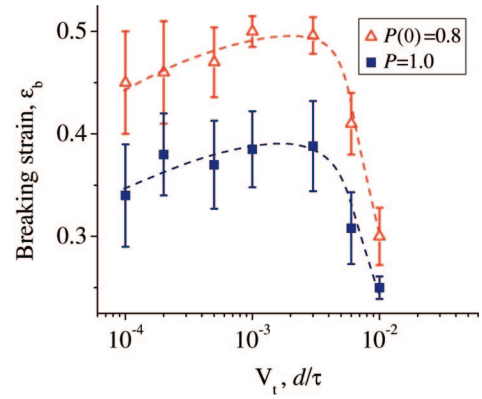

Figure 8. Dependence of the σ_b on tensile rate shown on a logarithmic scale for the largest sample at $P(0) = 0.8$ (red triangles) and $P = 1.0$ (blue squares).

sample, we define the saturation parameter $s = N_{labile}/N_{labile}^{(max)}$, which is the ratio of the number of formed labile bonds to the maximally permitted number of labile bonds in the sample. The total number of labile bonds is limited in the model by the total number of nodes on the surface of the gel particles (see Methodology). The dependence of s on ε for the $P = 0.8$ sample is plotted in the inset in Figure 7b. Initially, only approximately 28% of all possible labile bonds were formed in the sample; all the other labile bonds were sufficiently stressed that they underwent rupture, in accordance with the probability in eq 3. During the rearrangement in the sample, the number of labile bonds gradually increased and reaches $s \approx 0.5$ before the sample fractures.

On the other hand, the less reactive, stable bonds mostly just rupture (without re-forming) during the rearrangement for the $P = 1$ sample (see Figure 7a). As a consequence, the value of P, the ratio of the number of stable bonds to the total number of bonds, decreases from its initial value of $P = 0.8$ to $P \approx 0.53$ in the course of deformation, as shown in Figure 7b. These data support our contention that the re-forming of the labile bonds plays a crucial role in maintaining the stability of dual cross-linked samples.

Finally, we examined how the stability of the samples depends on V_t, the rate of the tensile deformation. Calculations were performed for rates V_t in the range from 10^{-4} through $10^{-2} \times d/\tau$. At a given rate, a stress−strain curve similar to that shown in Figure 6 was calculated for the largest sample with a randomly placed crack on its surface. The strain at which the sample fractures into two pieces, ε_b, was determined in each simulation as the strain at which the stress−strain curve drops sharply to zero. The results obtained for ε_b were averaged over eight independent simulations made with different positions of the crack. The results for the $P = 0.8$ and $P = 1.0$ samples are summarized in Figure 8. Points show the averaged values for ε_b, and the error bars mark the standard deviations. The plots reveal a maximum at a tensile rate of $V_t \sim 2 \times 10^{-3} \times d/\tau$ for both dual and permanently cross-linked

samples. (Note that a maximum in the dependence of ε_b on the tensile rate is known to occur for permanently cross-linked elastomers).[16] It is also evident from Figure 8 that, at any tensile rate, the ε_b calculated for the $P = 0.8$ sample is from ~20% (at fastest tensile rates $V_t \geq 6 \times 10^{-3} \times d/\tau$) to 30% (at slower tensile rates, $V_t < 6 \times 10^{-3} \times d/\tau$) higher than that for the $P = 1.0$ sample. This is in accordance with the results described above on the calculations at constant velocity. Note that it follows from Figure 8 that the stress−strain curves shown in Figure 6 are computed for conditions near the maximum of the ε_b (V_t) dependence.

CONCLUSIONS

In summary, we modeled the response of a cross-linked network of deformable gels to a tensile stress and found that the introduction of a small fraction of labile cross-links can dramatically improve the strength of the material. At present, there have been no experimental studies to explore the self-healing behavior of the nanogel material. Nonetheless, we can draw analogies with other experimental systems that indicate the validity of our predictions. For example, it is useful to recall the oligosulfide cross-linking molecules that contribute to the unique properties of vulcanized rubber.[17] In particular, the reshuffling of the labile S−S bonds as the rubber is deformed is what contributes to the toughness of this material.[18]

The behavior observed herein is also conceptually analogous to the properties that contribute to the strength of the abalone shell nacre, where brittle inorganic layers are interconnected by a layer of cross-linked polymers.[19] Under a tensile deformation, the weak cross-links or "sacrificial bonds" are the first to break. These ruptures dissipate energy and thereby mitigate the effects of the mechanical deformation. Consequently, the breakage of these sacrificial bonds helps maintain the structural integrity of the material.

Recently, researchers have shown that polymer chains that encompass a significant fraction of hydrogen bonds can also undergo a rapid structural rearrangement due to bond breaking and remaking that imparts self-healing properties to the bulk material.[9]

Our system combines aspects of the above examples. The labile bonds act as the "sacrificial" species, dissipating the energy of the applied deformation. Furthermore, the rapid re-forming of these bonds provides the structural rearrangement that preserves the mechanical integrity of the sample.

METHODOLOGY

Our approach for simulating the nanogel network is based on the lattice spring model (LSM),[20] where point-like masses (nodes) are interconnected by Hookean springs, which represent bonds. Figure 1a shows the 7-node model that represents the individual gel unit. These units are then interconnected into an extended material by both permanent and labile bonds.

Within a single gel unit, the nodes interact through a potential $U(r)$ that involves an attractive Hookean spring interaction and a repulsive force, which mimics an excluded volume around the node:

$$U(r) = \frac{\kappa}{2}\left(r^2 + \frac{a}{r}\right) \qquad (2)$$

with a cutoff distance r_c. Here, κ is the spring stiffness constant, r is the distance between the nodes, and a is the repulsion parameter. The equilibrium distance between the nodes is equal to $\Delta = (a/2)^{1/3}$. Within each gel unit, the bonds do not break during the course of the simulations.

To model bonds between gel units, we use the same interaction potential, which emanates from each of the surface nodes on the gel pieces. Now, however, the spring constant κ for the intergel interactions is taken to be six times weaker than that for intragel bonds. (While different values for the latter spring constants could be chosen, we note that for the large number of nodes considered here (in excess of 1000 for large samples), significant differences between the inter- and intragel spring constants can give rise to numerical instabilities.) Additionally, κ has the same value for stable and labile bonds. (The latter choice allowed us to specifically focus on isolating effects arising from the dual cross-linking.) In the case of a broken bond, the interaction potential is only given by the repulsive part (*i.e.*, by the term $\propto 1/r$ in eq 2).

The sample was prepared in two steps. In the first step, the hexagonal gel particles were arranged in the following manner; we examined three samples that encompassed five rows, with 10 particles in each row, eight rows with 10 particles in each row, and 12 rows with 15 particles in each row. The layers were constructed with lattice spacing 3Δ between the centers of the gel units, where Δ is the equilibrium distance between the nodes (2Δ is the horizontal size of the unit). The vertical spacing between the layers was equal to 1.3Δ. At this step, all possible bonds within the cutoff radius were established, and each node was allowed to subtend at most five interactions. All these interactions were marked as labile bonds. Then, the sample was equilibrated for 100 time steps (for the smallest sample) or 1000 time steps (for larger samples). During the equilibration, the initial mechanical stresses became relaxed and the most stressed bonds were ruptured in accordance with the probability in eq 3 below. In the second step, we specify the characteristics of each interparticle bond, assigning stable bonds with a probability P and labile bonds with a probability $(1 - P)$. Thus, even for a fixed value of P, each simulation has a different, independent distribution of stabile and labile bonds.

In this paper, we focus on the overall mechanical stability of the material and do not probe the details of the (fast) fracture processes that occurs at $\sigma > \sigma_{cr2}$. In particular, we take the dynamical behavior of our system to be in the overdamped limit, where we neglect the inertial terms in our equation of motion for the nodes. Thus, the velocity of a node is taken to be proportional to the net force acting on the node (where the net force is the sum of forces from neighboring nodes and from an external tensile force). We note that this assumption is commonly made in studies on gel dynamics.[21,22] Specifically, each gel node obeys the following dynamical equation: $d\mathbf{r}_i/dt = \mu\mathbf{F}_i$, where μ is the mobility and $\mathbf{F}_i$ is the force acting on node i. Here, we take μ to be a constant, and thus, we neglect the dependence of the mobility on the polymer density. The force acting on the node i is defined as follows $\mathbf{F}_i = -\partial U/\partial \mathbf{r}_i + \mathbf{F}_i^{ext}$, where the elastic energy U is equal to

$$U = \frac{1}{2}\sum_{m,n}{}' U_1(|\mathbf{r}_m - \mathbf{r}_n|)$$

The prime denotes that the summation is made at a given bond configuration at a particular moment of time, and $m \neq n$. The term $\mathbf{F}_i^{ext}$ is the external tensile force, which is applied to the nodes at the vertical edges of a rectangular sample. We numerically integrate these equations of motion (using the fourth order Runge−Kutta algorithm).

As explained above, in response to the applied deformation, the bonds between the gels units can rupture and reconnect. We adopted the Bell model[23] to describe the rupture and re-formation of bonds due to thermal fluctuations. The Bell model serves as a useful framework for describing the relationship between bond dissociation and stress[24] and has been widely used to describe the reversible bonds formed in proteins,[25] between biological cells or between cells and surfaces.[26−28] In accordance with the model,[23,27] the rupture rate, k_r, is an exponential function of the force applied to the bond

$$k_r^{(s,l)} = \nu^{(s,l)} \exp\left[\frac{r_0 F - U_0^{(s,l)}}{k_B T}\right] \quad (3)$$

Here $U_0^{(s,l)}$ is the potential well depth at zero mechanical stress, F is the applied force, r_0 is a parameter that characterizes change in the reactivity of the bond under stress, k_B is the Boltzmann constant, and T is the temperature. The parameter $\nu^{(s,l)}$ is an intrinsic frequency of an unstressed bond; in the lattice spring model, its value is equal to $\nu^{(s,l)} = \sqrt{\kappa/m}$, where κ is the bond stiffness and m is the reduced mass of the nodes attached to the bond. The superscripts s and l label stable and labile bonds, respectively. Taking representative values into consideration, we set the potential well depth equal to $U_0^{(l)} = 100 k_B T$ for labile bonds and $U_0^{(s)} = 140 k_B T$ for strong bonds.[29]

The re-forming rate, k_f, for a broken bond was calculated directly from the detailed balance principle[26,28]

$$\frac{k_r^{(s,l)}}{k_f^{(s,l)}} = \exp\left(-\frac{\Delta U^{(s,l)}}{k_B T}\right) \quad (4)$$

where $\Delta U^{(s,l)}$ is a difference in the potential energies of a connected and broken bond. The probability for a connected bond to break and the probability for a broken bond to re-form within a numerical time step Δt were taken to be of the following forms

$$w_r^{(s,l)} = 1 - \exp[-k_r^{(l,s)} \Delta t]$$
$$w_f^{(s,l)} = 1 - \exp[-k_f^{(l,s)} \Delta t] \quad (5)$$

Acknowledgment. Funding from the DOE (to A.C.B. and K.M. for financial support of G.V.K.) and ARO (to A.C.B.) is gratefully acknowledged.

REFERENCES AND NOTES

1. Wu, D. Y.; Meure, S.; Solomon, D. Self-Healing Polymeric Materials: A Review of Recent Developments. *Prog. Polym. Sci.* **2008**, *33*, 479–522.
2. Trask, R. S.; Williams, H. R.; Bond, I. P. Self-Healing Polymer Composites: Mimicking Nature to Enhance Performance. *Bioinsp. Biomim.* **2007**, *2*, P1−P9.
3. Balazs, A. C. Modeling Self-Healing Materials. *Mater. Today* **2007**, *10*, 18–23.
4. Hickenboth, C. R.; Moore, J. S.; White, S. R.; Sottos, N. R.; Baudry, J.; Wilson, S. R. Biasing Reaction Pathways with Mechanical Force. *Nature* **2007**, *446*, 423–427.
5. Oh, J. K.; Tang, C.; Gao, H.; Tsarevsky, N. V.; Matyjaszewski, K. Inverse Miniemulsion ATRP: A New Method for Synthesis and Functionalization of Well-Defined Water Soluble/Cross-Linked Polymeric Particles. *J. Am. Chem. Soc.* **2006**, *128*, 5578–5584.
6. Min, K.; Gao, H.; Yoon, J. A.; Wu, W.; Kowalewski, T.; Matyjaszewski, K. One-Pot Synthesis of Hairy Nanoparticles by Emulsion ATRP. *Macromolecules* **2009**, *42*, 1597–1603.
7. Oh, J. K.; Drumright, R.; Siegwart, D. J.; Matyjaszewski, K. The Development of Microgels/Nanogels for Drug Delivery Applications. *Prog. Polym. Sci.* **2008**, *33*, 448–477.
8. Tsarevsky, N. V.; Min, K.; Jahed, N. M.; Gao, H.; Matyjaszewski, K. Degradable Polymers and Materials–Principles and Practice. *ACS Symp. Ser.* **2006**, *939*, 184–200.
9. Cordier, P.; Tournilhac, F.; Soulie-Ziakovic, C.; Leibler, L. Self-Healing and Thermoreversible Rubber from Supramolecular Assembly. *Nature* **2008**, *451*, 977–980.
10. Deplace, F.; Rabjohns, M. A.; Yamaguchi, T.; Foster, A. B.; Carelli, C.; Lei, C.-H.; Ouzineb, K.; Keddie, J. L.; Lovell, P. A.; Creton, C. Deformation and Adhesion of a Periodic Soft−Soft Nanocomposite Designed with Structured Polymer Colloid Particles. *Soft Matter* **2009**, DOI: 10.1039/b815292f.
11. Budinski, K. G.; Budinski, M. K. *Engineering Materials: Properties and Selection*, 8th ed.; Prentice Hall: Columbus, 2004.
12. Lawn, B. R. *Fracture of Brittle Solids*, 2nd ed.; Cambridge University Press: New York, 1993.
13. Dirama, T. E.; Varshney, V.; Anderson, K.; Shumaker, J. A.; Johnson, J. A. Coarse-Grained Molecular Dynamics Simulations of Ionic Polymer Networks. *Mech. Time-Depend. Mater.* **2008**, *12*, 205–220.
14. Tsige, M.; Lorentz, C. D.; Stevens, M. J. Role of Network Connectivity on the Mechanical Properties of Highly Cross-Linked Polymers. *Macromolecules* **2004**, *37*, 8466–8472.
15. Mukherji, D.; Abrams, C. F. Microvoid Formation and Strain Hardening in Highly Cross-Linked Polymer Networks. *Phys. Rev E* **2008**, *78*, 050801(R) .
16. Gents, A. N. Strength of Elastomers. In *Science and Technology of Rubber*; 2nd ed.; Mark, J. E., Erman, B., Eirick, F. R., Eds.; Academic Press: New York, 1994.
17. Tobolsky A. V.; MacKnight, W. J. *Polymeric Sulfur and Related Polymers*; Wiley: New York, 1966.
18. Aklonis, J. J.; MacKnight, W. J. *Introduction to Polymer Viscoelasticity*, 2nd ed.; Wiley-Interscience: New York, 1983.
19. Smith, B. L.; Schaffer, T. E.; Viani, M.; Thompson, J. B.; Frederick, N. A.; Kindt, J.; Belcher, A.; Stucky, G. D.; Morse, D. E.; Hansma, P. K. Molecular Mechanistic Origin of the Toughness of Natural Adhesives, Fibres and Composites. *Nature* **1999**, *399*, 761–763.
20. Buxton, G. A.; Balazs, A. C. Modeling the Dynamic Fracture of Polymer Blends Processed Under Shear. *Phys. Rev. B* **2004**, *69*, 054101.
21. Yashin, V. V.; Balazs, A. C. Pattern Formation and Shape Changes in Self-Oscillating Polymer Gels. *Science* **2006**, *314*, 798–801.
22. Kuksenok, O.; Yashin, V. V.; Balazs, A. C. Mechanically Induced Chemical Oscillations and Motion in Responsive Gels. *Soft Matter* **2007**, *3*, 1138–1144.
23. Bell, G. I. Models for the Specific Adhesion of Cells to Cells. *Science* **1978**, *200*, 618–627.
24. Chang, K. C.; Tees, D. F. J.; Hammer, D. A. The State Diagram for Cell Adhesion under Flow: Leukocyte Rolling and Firm Adhesion. *Proc. Natl. Acad. Sci. U.S.A.* **2000**, *97*, 11262–11267.
25. Wiita, A. P.; Ainavarapu, S. R. K.; Huang, H. H.; Fernandez, J. M. Force-Dependent Chemical Kinetics of Disulfide Bond Reduction Observed with Single-Molecule Techniques. *Proc. Natl. Acad. Sci. U.S.A.* **2006**, *103*, 7222–7227.
26. Bell, G. I.; Dembo, M.; Bongrand, P. Competition Between Nonspecific Repulsion and Specific Bonding. *Biophys. J.* **1984**, *45*, 1051–1064.
27. King, M. R.; Hammer, D. A. Multiparticle Adhesive Dynamics: Hydrodynamic Recruitment of Rolling Leukocytes. *Proc. Natl. Acad. Sci. U.S.A.* **2001**, *98*, 14919–14924.
28. Bhatia, S. K.; King, M. R.; Hammer, D. A. The State Diagram for Cell Adhesion Mediated by Two Receptors. *Biophys. J.* **2003**, *84*, 2671–2690.
29. Sanderson, R. T. *Chemical Bonds and Bond Energy*. Academic Press: New York, 1976.